Taylor & Francis
Taylor & Francis Group

Journal of Asian Architecture and Building Engineering

ISSN: (Print) (Online) Journal homepage: https://www.tandfonline.com/loi/tabe20

Mechanical Properties of Film-bag Sand Cofferdam: Theoretical Analysis and Numerical Study

Bo Feng, Chun-yuan Zhang, Xing-jin Wang & Yong-jiu Qian

To cite this article: Bo Feng, Chun-yuan Zhang, Xing-jin Wang & Yong-jiu Qian (2023): Mechanical Properties of Film-bag Sand Cofferdam: Theoretical Analysis and Numerical Study, Journal of Asian Architecture and Building Engineering, DOI: 10.1080/13467581.2023.2165882

To link to this article: https://doi.org/10.1080/13467581.2023.2165882

Publisher: Taylor & Francis & The Author(s). Published by Informa UK Limited, trading as Taylor & Francis Group on behalf of the Architectural Institute of Japan, Architectural Institute of Korea and Architectural Society of China.

Journal: *Journal of Asian Architecture and Building Engineering*

DOI: 10.1080/13467581.2023.2165882

Mechanical Properties of Film-bag Sand Cofferdam: Theoretical Analysis and Numerical Study

Bo Feng*, Chun-yuan Zhang, Xing-jin Wang, Yong-jiu Qian

Department of Bridge Engineering, Southwest Jiaotong University, Chengdu 610031 P.R.China;

ABSTRACT

To study the mechanical properties of the membrane bag sand cofferdam under the action of geotextile hoop during the construction, the theoretical derivation of the film-bag sand enhancement mechanism was carried out firstly. Based on the construction cofferdam project of Cao Fei-Dian Nacho River 2# Bridge in Tangshan City, a finite element model of sandbag and sand blowing cofferdam with measured material parameters was established based on the ANSYS platform, and then different pipes were used to calculate the bag height under self-weight and external load, and the variation law of self-weight and external load, as well as the sand blowing cofferdam under different concrete slab thickness was analyzed. The main conclusions include: (1) The relationship between the height of the membrane sandbag and the tensile force of the soil sandbag is proposed, the relationship between the shape of the sandbag and its weight and the external load is further deduced. (2) The axial tension of the type bag is proportional to the quadratic of the height of the type bag sand without

Bo Feng, Corresponding author*, Department of Bridge Engineering, Southwest Jiaotong University, Chengdu 610031, P.R.China. E-mail: Fengboswjt@163.com; Tel: +86 18602837305. Orcid ID: https://orcid.org/0000-0003-0887-6085.
Chun-yuan Zhang, Master student, Department of Bridge Engineering, Southwest Jiaotong University, Chengdu 610031, P.R.China. E-mail:409160232@qq.com;
Xing-jin Wang, Engineer, CHUANJIAN Institute Ofinvestigation and Design, Chengdu 610031, P.R.China. E-mail:695701334@qq.com
Yong-jiu Qian, Ph.D., Professor., Department of Bridge Engineering, Southwest Jiaotong University, Chengdu 610031, P.R.China. E-mail: 1991265426@qq.com.

considering the friction condition, which is consistent with the theoretical equation. (3) As the concrete slab thickness increases, the vertical settlement of the blown sand cofferdam gradually decreases under the action of the cast-in-place bracket, and the reduction of the uneven settlement in the cross-bridge direction is greater than that of the vertical settlement.

Keywords: Film bag sand; Sand-blown Cofferdam; Mechanical properties; Shear strength; ANSYS platform

1. INTRODUCTION

With the gradual exploration of the marine environment, China's marine engineering construction has been gradually strengthened, and the construction technology in various marine environments has been continuously developed, among which the land-blowing technology has also been developed significantly. In the construction of coastal ports, submarine tunnels, cross-sea bridges, and other projects, it is often necessary to build temporary enclosure structures before the main project construction. The Sand-blown cofferdams are widely used in the construction of temporary cofferdams in near-shore harbors and wharves of rivers, lakes, and seas due to their advantages of convenient construction, less pollution, high mechanization, and easy dismantling (Kang et al. 2020). According to the filling materials, the traditional cofferdams can be divided into earth and stone, wooden cage, sheet pile lattice, reinforced concrete, timber sheet pile as well as pile wall frame structure cofferdams (Xue et al. 2020; Wang et al. 2020).

In recent years, under the conditions of large areas of sea reclamation and land reclamation projects, poor foundation mechanical indicators, rapid project progress, and complex

construction environments such as waves and typhoons lead to cofferdams construction more and more difficult (Xiu et al. 2021; Li et al. 2018), especially for traditional earth-rock cofferdams or concrete cofferdams. R ecently, the film bag sand cofferdam technology has been popularized and applied. For the problem of foundation deformation and bearing capacity under the action of flexible loads caused by deep offshore soft soil and low bearing capacity of the foundation, some scholars have carried out related research works (Zhou et al. 2017). Membrane bag sand cofferdam technology is a kind of cofferdam construction technology, which uses synthetic geomembrane bag material and hydraulic power to build and form cofferdam layer by layer according to design requirements (Liu et al. 2020). Compared with the traditional concrete cofferdam, the film-bag sand cofferdam has the following advantages: (1) The construction technology of water conservancy filling has a high degree of mechanization and fast construction speed; (2) The film-bag sand cofferdam, as a flexible foundation, can adapt to deformation of soft soil foundation; (3) The membrane bag is mainly made of synthetic fibers such as the polyester, nylon, and polypropylene, which have strong anti-burial and corrosion resistance; (4) The geomembrane bag is permeable to water and sand and has good filtration. The isolation function can be adapted to the underwater construction of the offshore cofferdam; (5) The filling material of the membrane bag sand cofferdam can be obtained locally. The production of geosynthetics is very mature and the total cost is low. To improve the construction efficiency and overall stability of the membrane bag sand cofferdam project, the membrane bag sand cofferdam technology has been continuously developed. Among them, the size expansion of the geomembrane bag is a prominent development, forming a large-size membrane bag sand cofferdam. The length of

the geomembrane bag can reach hundreds of meters and the width is tens of meters.

Up to now, Membrane bag sand cofferdam technology has been rapidly promoted, and there have been many successful engineering applications in the world. Firstly, Restall et al. (2002) summarized the successful application of geomembrane bag sand technology in several projects such as Green Island, Gold coast Broadwater and North Kirra Groyne in Australia. His investigation indicated that geomembrane bags have a wide range of applications and can be applied to different geomembrane bag materials and forms according to local conditions in scouring surfaces, slope protection embankments, cut-off ditches, artificial reefs, and other projects. Saathoff et al. (2007) summarized the utilized of geomembrane bags at the areas such as Australia and Germany in scouring surfaces, coastal erosion protection, seawalls, and sand reinforcement, stating that geomembrane bag sand technology provides a flexible, economical, and environmentally friendly solution for the above projects and has become an important technical component in offshore engineering.

The NAJMAT project on Reem Island in Abu Dhabi, United Arab Emirates (Yang et al. 2009) used a film bag sand cofferdam to build a temporary cofferdam at the port to provide dry construction conditions for the project through continuous precipitation. During the construction process, it was found that after the cofferdam construction was completed, there was a triangular seam between the sandbags of the main cofferdam, resulting in serious water leakage. For this reason, another sub-cofferdam was built inside the main cofferdam. The project concluded that in the film bag sand cofferdam, the length of the individual sandbag should be increased to reduce the number of overlaps of the cofferdam body and reduce the

triangular seam, thereby improving the anti-seepage capability. At the same time, a reasonable thickness of the film bag sand should be selected in the engineering design, the filling time of each sandbag cuff should be controlled, and the flatness of the film bag sand should be maintained during construction.

In China, the engineering application of the membrane bag sand cofferdam first appeared in 1974. In the slope protection project of the Sui Ma-wan bend of the Yangtze River in Jiangsu Province. The polypropylene woven cloth, polyvinyl chloride rope net, and concrete blocks were used to make soft sinkers instead of traditional throwing stone footguards (Zhou et al. 2014). In the following 40 years, the geomembrane bag sand construction technology has been innovated and developed continuously in China, and it has been widely used in engineering applications such as sea reclamation, embankment engineering, and deep-water channel treatment engineering throughout the country. In 1992, the cofferdam filling project of Ship Sewage Treatment Plant (SSTP) in Shanghai was constructed (Li et al. 2019), the large-size membrane bag sand cofferdam technology was used as a permanent structure in the above offshore projects. As well as the large-size geomembrane bag combined with the mud pump filling technology was illustrated to improve the quality of the embankment. After being built, it has experienced typhoon hazards and it operated well, indicating that the large-size film bag sand cofferdam has good durability.

Binhai New Area of Tianjin, China, the world's largest reclamation projects was carried out in this area. The planned land reclamation area is about 500 square kilometers, the large-size film bag sand cofferdam has been widely used in this area and the cofferdam technology has

developed rapidly (Liu et al. 2016; Peng et al. 2018). It took five years to complete the cofferdam with a total length of nearly 70 kilometers and a sea area of 37.8 km^2 in the Lingang Industrial Zone of Tianjin.

On the other hand, a large number of engineering practices have put forward new ideas for the traditional film bag sand. For example, Chen et al. (2016) conducted a centrifugal model test of a sandbag cofferdam on a natural soft foundation and a plastic drainage board foundation for a sea reclamation project in Tianjin. Sandbag cofferdam combined with plastic drainage board has strong applicability in sea reclamation projects. Among them, the geotextile plays the role of reinforcement, which limits the horizontal displacement of the cofferdam. The plastic drainage board accelerates the foundation consolidation and drainage, effectively improving the strength of the soft foundation during the cofferdam construction process, and enhancing the stability of the sandbag cofferdam. Then, Matsuoka et al. (2003) studied the deformation characteristics of the bagged sand cofferdam and explored the ultimate compressive strength and its main influencing factors under the vertical load of the geotechnical bagged sand.

The soil seepage failure problem within a cylindrical cofferdam has been numerically investigated by Benmebarek et al.（2022） in axisymmetric groundwater flow conditions without simplifying assumptions. In addition, the effects of the cofferdam radius and various parameters of soil and interface were taken into account in this analysis. The Numerical computations of the H_C/D critical values and seepage failure modes of homogenous cohesionless sandy soils within a cylindrical cofferdam have been performed using the FLAC

code for various scenarios.

In order to study the wave/current-induced seabed stability around a cofferdam, the hydrodynamic response and seabed response around the dumbbell cofferdam under combined wave and current loading are studied by Chen and Jeng (2022) via the numerical investigation. The numerical results conclude that: The current has a significant effect to the hydrodynamic response around the dumbbell cofferdam. The dumbbell cofferdam can obviously affect the influence of the current on the pore-water pressures. In the back of the cofferdam, an obvious mutation point appears in the influence trend of the current on the pore-water pressures at the embedded depth, as well as the liquefaction zone can be expanded as the following current is superimposed on the wave load.

Lu et al. (2023) investigated the failure mechanism of nonuniform large geotextile-reinforced cofferdam under seepage and excavation effects on soft sediments. A numerical model was established and validated with available testing results. Then, parametric studies were carried out to investigate the potential influence factors. This study found that the difference between the upstream and downstream water levels and the excavation depth both have significant influences on the stability of cofferdams.

The cofferdam technology is currently used in many offshore new construction projects, and many of them made cofferdam as a cast-in-suit support foundation. However, there are few studies on sand-blown cofferdam as the foundation of cast-in-suit bridges up to now, and few connecting between engineering construction and theoretical research, so it is necessary to

systematically study the mechanical properties of sand-blown cofferdams. Given the existing problems of sand-blown cofferdam as the foundation of the cast-in-suit bridge, this investigation starts from the following three main objects, which are: (1) The overall strength enhancement theory of the molded sand under the geotextile hoop action; (2) The influence of the post-cast concrete slab and the steel cushion beam stiffness of the sand-blown cofferdam on the settlement, (3) The influence of the settlement of the cofferdam on the construction of the cast-in-suit bridge and the stress condition of the completed bridge.

2. STRENGTHENING MECHANISM OF FILM-BAG SAND

The sand body is a loose aggregate of sand particles, and the essential source of its strength is mainly through the friction between the sand particles. When the outside of the sand body is wrapped by the film bag, the film bag will deform the axis under the action of the filling internal pressure and the sand self-weight load. The friction law shows that the friction force increases between the sand particles so that the overall strength of the film bag sand is improved. For cohesive soils, soil cohesion is mainly caused by intermolecular forces and the binding attraction generated by the hydrogen bond interaction between soil particles and colloids produced under the joint action of cohesion. The non-cohesive sand is similar to the reinforcement of the geomembrane bag, the contact pressure between soil particles increases, as well as the overall strength of the film bag sand increases.

2.1 The ultimate strength of clayey soil filled with membrane bag

At present, the common failure criteria in geotechnical research are the Cambridge model, generalized Mises criterion, Moore-Coulomb theory, as well as the Lade-Duncan model (Pei et al.

2018). When the sand body in the film bag sand is in the limit state under the action of external and self-weight load, its total stress should satisfy the above several failure criteria. Different failure criteria will result in different accuracy results. According to the Moore-Coulomb strength theory, when a certain point in the soil reaches the limit equilibrium state, which can be expressed as:

$$\frac{(\sigma_1-\sigma_3)}{2}=\frac{(\sigma_1+\sigma_3)}{2}\sin\varphi+c\cos\varphi \quad (1)$$

Then, Equation (1) can be written as:

$$\sigma_1=\frac{1+\sin\varphi}{1-\sin\varphi}\sigma_3+2c\frac{\cos\varphi}{1-\sin\varphi} \quad (2)$$

Making the $\frac{1+\sin\varphi}{1-\sin\varphi}=K_p$, which is expressed by the coefficient of passive earth pressure. According to the relationship of a trigonometric function $\frac{\cos\varphi}{1-\sin\varphi}=\sqrt{K_p}$. Equation (2) can be expressed as:

$$\sigma_1=\sigma_3K_p+2c\sqrt{K_p} \quad (3)$$

For the membrane bag sand due to the existence of the external membrane bag of the hoop effect, the limit equilibrium state of the sand body (Figure 1) is expressed as follow, where T denotes the tension force.

$$\sigma_1'+\frac{2T}{B}=(\sigma_3'+\frac{2T}{H})K_p+2c\sqrt{K_p} \quad (4)$$

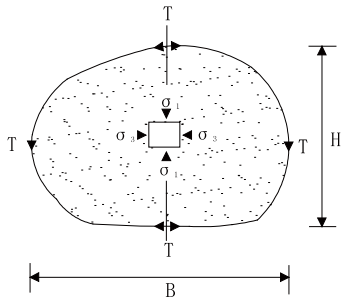

Fig. 1 The equivalent calculation diagram of film-bag sand

Then, Equation (4) can be written as:

$$\sigma_1' = \sigma_3' K_p + 2\frac{T}{B}\left(\frac{B}{H}K_p - 1\right) + 2c\sqrt{K_p} \tag{5}$$

Bring Formula (5) into Formula (3) to obtain:

$$\sigma_3 K_p + 2c\sqrt{K_p} = \sigma_3' K_p + 2\left[\frac{T}{B\sqrt{K_p}}\left(\frac{B}{H}K_p - 1\right) + c\right]\sqrt{K_p} \tag{6}$$

Among them, c is the cohesion of the sand body in the film bag, φ is the internal friction angle of the sand body, and B、H and L are the width, height, and length of the sandbag, respectively.

From the above two types, it can be seen that the hoop effect of the geotechnical sandbag provides an additional cohesion c_f to the internal sand body, which is:

$$c_f = \frac{T}{B\sqrt{K_p}}\left(\frac{B}{H}K_p - 1\right) \tag{7}$$

At this time, the internal cohesion of the sand body is as follows:

$$C = \frac{T}{B\sqrt{K_p}}\left(\frac{B}{H}K_p - 1\right) + c = c_f + c \tag{8}$$

According to Mohr-Coulomb's theory, the shear strength of clayey soil is as follows:

$$S = c + \sigma \tan\varphi \tag{9}$$

When the type of sand is fixed, its corresponding internal friction angle can be determined, and internal friction value has nothing to do with the external load, so when there is a hoop of the film bag, the shear strength moves on the s line, which was shown in Figure 2.

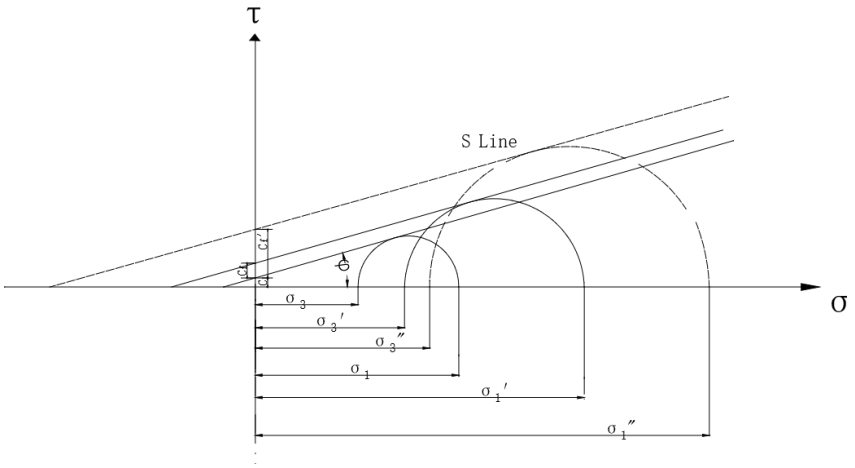

Fig. 2 Mohr-Coulomb strength line of reinforced sand filled with membrane bag

Among them, σ denotes the normal stress acting on the shear plane in the sand. The shear strength of reinforced film bag can be expressed as:

$$S = C + \sigma' \tan\varphi = c + c_f + \sigma' \tan\varphi = \left[\frac{\sigma_1' - \sigma_3'}{2} + \frac{T(B-H)}{HB} \right] \cos\varphi \qquad (10)$$

For clayey soil, when a point in the soil reaches the limit equilibrium state, which can be expressed as:

$$\sigma_1 = \sigma_3 \tan^2(45° + \frac{\varphi}{2}) + 2c \tan(45° + \frac{\varphi}{2}) \qquad (11)$$

$$\sigma_3 = \sigma_1 \tan^2(45° - \frac{\varphi}{2}) - 2c \tan(45° - \frac{\varphi}{2}) \qquad (12)$$

Take the Equation (11) into the (12) and arrange it like this:

$$\sigma_1 - \sigma_3 = \sigma_1[1 - \tan^2(45° - \frac{\varphi}{2})] + 2c \tan(45° - \frac{\varphi}{2}) \qquad (13)$$

Usually, the maximum principal stress σ_1 is the vertical compressive stress, which can be expressed as $\sigma_1 = \gamma H$, γ is the weight of the soil, and H is the buried depth. Therefore, the film bag sand strengthens the ultimate shear strength of the thick soil:

$$S=\left\{\frac{1}{2}[\gamma H(1-\tan^2(45°-\frac{\varphi}{2}))+2c\tan(45°-\frac{\varphi}{2})]+\frac{T(B-H)}{HB}\right\}\cos\varphi \quad (14)$$

2.2 Ultimate strength of non-cohesive soil filled with membrane bag

For sandy soil, the cohesion is zero. According to the Moore-Coulomb theory, when a certain point inside the sand body reaches the limit equilibrium state:

$$\frac{1}{2}(\sigma_1\text{-}\sigma_3)=\frac{1}{2}(\sigma_1+\sigma_3)\sin\varphi \quad (15)$$

$$\sigma_1=\frac{1+\sin\varphi}{1-\sin\varphi}\sigma_3=\sigma_3K_p \quad (16)$$

The inner limit equilibrium state of the film bag sand under the action of the outer film bag hoop can be expressed as:

$$\sigma_1'+\frac{2T}{B}=(\sigma_3'+\frac{2T}{H})K_p \quad (17)$$

Furtherly,

$$\sigma_1'=\sigma_3'K_p+2\frac{T}{B}(\frac{B}{H}K_p-1) \quad (18)$$

On the other hand, the shear strength is:

$$S=\sigma'\tan\varphi=\sigma'\tan\varphi=\left[\frac{\sigma_1'\text{-}\sigma_3'}{2}+\frac{T(B-H)}{HB}\right]\cos\varphi \quad (19)$$

For non-cohesive soil, when a point in the soil reaches the limit equilibrium state σ_1 and σ_3 can be expressed:

$$\sigma_1=\sigma_3\tan^2(45°+\frac{\varphi}{2}) \quad (20)$$

$$\sigma_3=\sigma_1\tan^2(45°-\frac{\varphi}{2}) \quad (21)$$

$$\sigma_1 - \sigma_3 = \sigma_1[1 - \tan^2(45° - \frac{\varphi}{2})] \quad (22)$$

Similarly, the first principal stress can also be expressed as: $\sigma_1 = \gamma H$, The Equation(14) can also be written as follows:

$$S = [\frac{1}{2}\gamma H(1 - \tan^2(45° - \frac{\varphi}{2})) + \frac{T(B-H)}{HB}]\cos\varphi \quad (23)$$

3. THEORETICAL DERIVATION OF ULTIMATE BEARING CAPACITY OF FILM-BAG SAND

3.1 The relationship between the strength of film-bag sand and the height of tube bag

It is assumed that under the vertical external load, the shape of the pipe bag sand is shown in Figure 3, and in which the friction between the bag wall and the sand body is ignored.

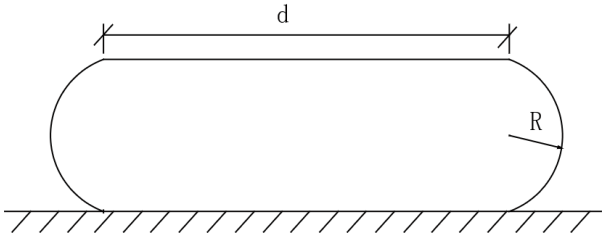

Fig. 3 Approximate picture of film bag sand

If the total length of the bag is L, then:

$$L = 2d + 2\pi R \quad (24)$$

Thus, the volume of bag can be expressed:

$$S = \pi R^2 + 2dR \quad (25)$$

And the sand filling rate of tube bags is:

$$w_0 = \frac{4\pi S}{L^2} = \frac{4\pi RL - 4\pi^2 R^2}{L^2}, \quad 0 < w_0 < 1 \quad (26)$$

In which:

$$R^2 - \frac{RL}{\pi} + \frac{w_0 L^2}{4\pi^2} = 0 \tag{27}$$

$$R = \frac{L}{2\pi}(1 \pm \sqrt{1 - w_0}) \tag{28}$$

When the sand filling rate of the tube bag is constant, the shape of the tube bag can be determined. Assuming that the friction between the inner wall of the tube bag and the sand is not considered, according to the balance condition of the circumferential tension of the tube bag and the lateral extrusion force of the sand, the calculation diagram of membrane bag balance under the dead weight load is presented in Figure 4 , we can get (Lambe et al. 1991):

$$\begin{aligned} 2T &= \int_0^{\pi} \rho g R(R + R\cos\theta)\sin\theta d\theta \\ &= \rho g R^2 \int_0^{\pi} (\sin\theta + \frac{\sin 2\theta}{2}) d\theta = 2\rho g R^2 \end{aligned} \tag{29}$$

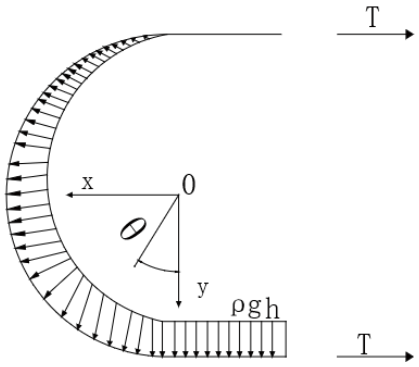

Fig. 4 Calculation diagram of membrane bag balance under the dead weight load

Then, the calculation diagram of membrane bag balance under dead weight and external load is shown in Figure 5,

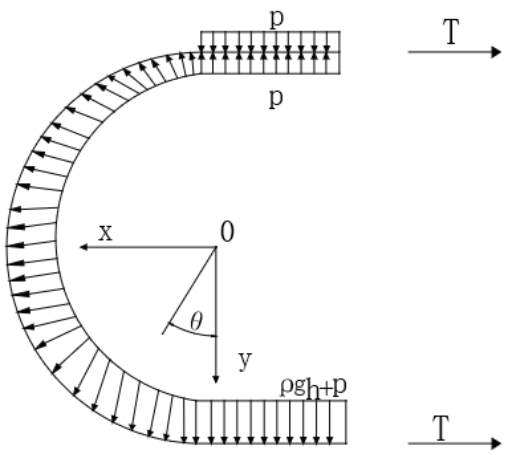

Fig. 5 Calculation diagram of membrane bag balance under dead weight and external load

Therefore, the circumferential tension of the bag can be obtained under dead weight load:

$$T = \rho g R^2 \tag{30}$$

When there is a vertical load on the bag:

$$\begin{aligned} 2T &= \int_0^{\pi} [\rho g(R + R\cos\theta) + pR] R d\theta \sin\theta \\ &= \rho g R^2 \int_0^{\pi} (\sin\theta + \frac{\sin 2\theta}{2}) d\theta + pR \int_0^{\pi} \sin\theta d\theta = 2\rho g R^2 + 2pR \end{aligned} \tag{31}$$

Therefore, the circumferential tension of the tube bag can be obtained under the external load:

$$T = \rho g R^2 + pR \tag{32}$$

It can be seen that in the ideal state, that is, regardless of the friction between the tube bag and the sand, the shape of the tube bag is a rectangle add a circle. When the sand filling rate of the tube bag is constant, the shape of the tube bag can be determined.

The external load that the sand-filled body can bear at this time can also be determined:

$$p = \frac{T}{R} - \rho g R \tag{33}$$

However, in engineering practice, under the action of dead weight and geotextile bag hoop, the shape of film bag sand is quasi-ellipsoidal, as shown in Figure 6, rather than the idealized model assumed above.

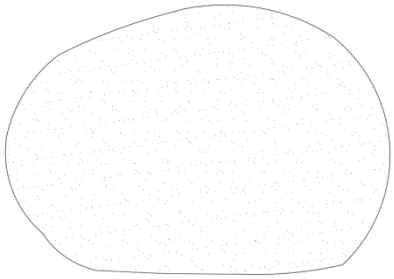

Fig. 6 Approximate of the actual shape of film bag sand

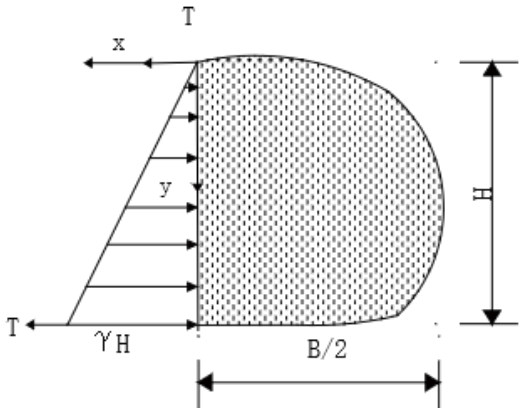

Fig. 7 Calculation diagram of actual shape balance of film bag sand

At this point, the calculation graph is shown in the following Figure 7, in which:

$$2T = \gamma \int_0^H h dh = \gamma \frac{H^2}{2} \tag{34}$$

Under the action of internal pressure and external load (Figure 8):

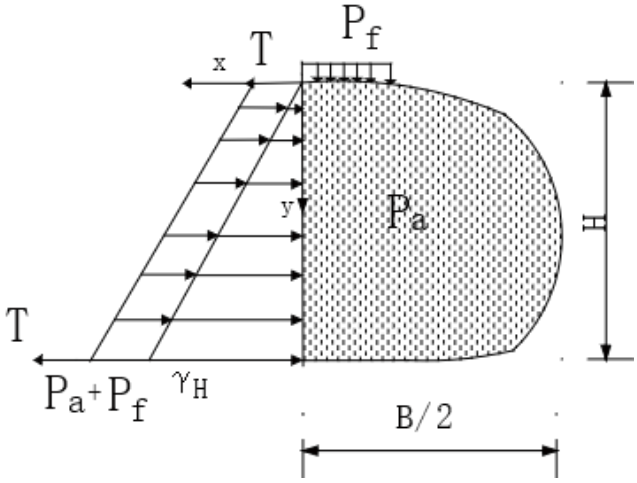

Fig. 8 Calculation diagram of actual shape balance of dead weight and internal and external load

At this point:

$$2T = \int_0^H \left[(P_a + P_f) + \gamma h \right] dh = \gamma \frac{H^2}{2} + (P_a + P_f) H \quad (35)$$

$$T = \gamma \frac{H^2}{4} + \frac{1}{2}(P_a + P_f) H \quad (36)$$

Among them, P_a is the filling pressure, P_f which is the external load to convert the vertical pressure. At this time, the cohesion of film bag sand can be approximately expressed by the height of the bag as follows:

$$C = \frac{\gamma \frac{H^2}{4} + \frac{1}{2}(P_a + P_f) H}{B\sqrt{K_p}} (\frac{B}{H} K_p - 1) + c \quad (37)$$

Compared with formulas 30 and 35 $H \approx 2R$, we can see that the results obtained by the two methods are the same.

Bring formula 35 into 14 and 23, respectively, and get the following formulas:

$$S = \frac{1}{2}\left\{ [\gamma H (1 - \tan^2(45° - \frac{\varphi}{2})) + 2c \tan(45° - \frac{\varphi}{2})] + (P_a + P_f)(1 - \frac{H}{B}) \right\} \cos\varphi \quad (38)$$

$$S = \frac{1}{4}[2\gamma H (1 - \tan^2(45° - \frac{\varphi}{2})) + \gamma H^2 + 2(P_a + P_f)(1 - \frac{H}{B})] \cos\varphi \quad (39)$$

3.2 Relationship between the shape of film-bag sand and internal and external load

Worldwide scholars have done much-related research about the relationship between the shape of film-bag sand and internal and external load (Matsuoka et al. 2006; Guo et al. 2011; Plaut et al. 1999; Malik et al. 2011; Namias et al. 1985), but almost all research is based on the two thin-film theories and the medium continuity theory. Liu et al. (2010) conducted relevant experimental research and found that the drainage process of pipe bag sand is very short, and the shape of the pipe belt hardly changes under non-water immersion conditions. However, in the process of static drainage, the volume sand filling rate and water-sand ratio in the pipe belt change non-linearly at any time, and the complexity of the boundary conditions makes the research on the pipe belt more complicated. Considering that the shape of the pipe strip before and after drainage is almost the same, the relationship between the internal pressure of the film bag sand and the shape of the pipe

strip during the filling process is now theoretically derived. The following assumptions are made before the theoretical derivation:

(1) Assumption of plane strain: the length direction of the pipe strip is much larger than the width direction;

(2) Assumption of small deformation: it is assumed that the deformation of the geotextile tape in the axial direction is small and can be ignored;

(3) The foundation is straight and rigid.

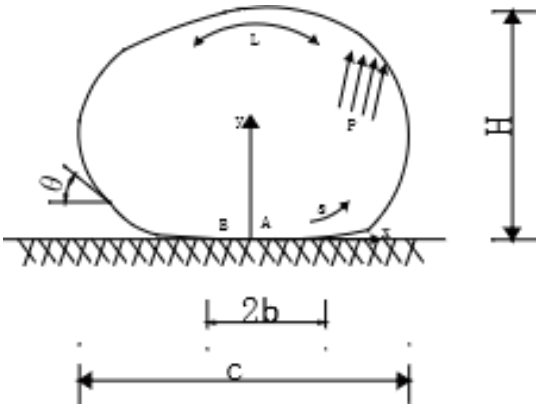

Fig. 9 calculation diagram of film bag sand shape

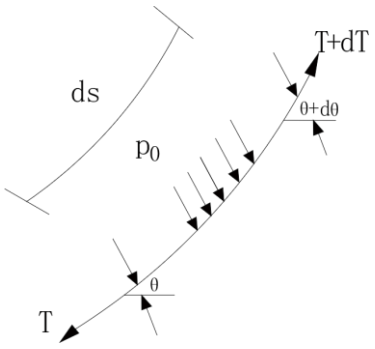

Fig. 10 Calculation diagram of tube bag micro-segment

As shown in Figure 9, L denotes the perimeter of the tube belt, S denotes the length from the starting point of foundation to the calculated section, θ denotes the angle between the tangent and the horizontal direction of the pipe, B is the contact length between the pipe belt and the rigid foundation, C is the transverse width of the tube band, P is the conversion pressure of filling

internal pressure and sand body weight acting on the inner wall of tube bag.

The micro-segment tube band is shown in Figure 10, and the pressure value at a certain point corresponding to the actual vertical position y of the filling process is as follows:

$$P = P_0 + \gamma y \tag{40}$$

According to the static equilibrium relationship between the two directions, the following Equation (40) and (41) can be obtained:

$$\sum Fx = 0 : (T + dT)\cos(\theta + d\theta) - T\cos\theta + P\sin(\theta + \frac{d\theta}{2})ds = 0 \tag{41}$$

$$\sum Fy = 0 : (T + dT)\sin(\theta + d\theta) - T\sin\theta - P\cos(\theta + \frac{d\theta}{2})ds = 0 \tag{42}$$

Expand Equation (40) to get:

$$(T + dT)(\cos\theta\cos d\theta - \sin\theta\sin d\theta) - T\cos\theta + P(\sin\theta\cos\frac{d\theta}{2} + \cos\theta\sin\frac{d\theta}{2})ds = 0 \tag{43}$$

According to the properties of a trigonometric function, it can be approximated as follows:

$$(T + dT)(\cos\theta - d\theta\sin\theta) - T\cos\theta + Pds(\sin\theta + \frac{d\theta}{2}\cos\theta) = 0 \tag{44}$$

Omitting the higher-order infinitesimal terms $dTd\theta$、$dsd\theta$ inverse:

$$dT\cos\theta - Td\theta\sin\theta + Pds\sin\theta = 0 \tag{45}$$

Reorganized:

$$\frac{dT}{ds}\cos\theta - \frac{T}{ds}d\theta\sin\theta + P\sin\theta = 0 \tag{46}$$

$$\frac{dT}{ds}\sin\theta + \frac{T}{ds}d\theta\cos\theta - P\cos\theta = 0 \tag{47}$$

For the entire tube with:

$$\oint Tds = 0; \oint (T\theta_S - P)ds = 0 \tag{48}$$

When the friction between the filling sand and the bag is ignored, the bag has the same tensile force in the extended circumferential direction, that is $dT = 0$. At this point, Equation (45) and (46) can be expressed as:

$$Td\theta = Pds \tag{49}$$

For tube with micro-segments， in which:

$$\begin{cases} ds = \sqrt{dx^2 + dy^2} = \sqrt{1 + y'^2}dx \\ \dfrac{dx}{ds} = \cos\theta \\ \dfrac{dy}{ds} = \sin\theta \\ y' = \dfrac{dy}{dx} = \tan\theta \\ t_S = 0 \\ t\theta_S - P = 0 \end{cases} \tag{50}$$

When the foundation is a straight rigid foundation, the contact length 2b between the bag and the foundation can be obtained according to the static equilibrium condition.

$$2b(P_0 + \gamma H) = W; b = \frac{W}{2(P_0 + \gamma H)} \tag{51}$$

W is the bag filling weight.

$$S = \int_0^y \sqrt{1 + (x'(y))^2}dy \tag{52}$$

Where θ_0 is the tangential angle of the foundation at the beginning of the separation between the bag and the foundation. When the ground is a flat rigid foundation, the boundary conditions can be obtained:

$$\theta(0) = 0, \theta(b) = \theta_0, \quad \theta_0 = 0 \tag{53}$$

The tangent angle of a calculated position of the tube bag can be approximately written as a first-order function related to the cumulative arc length:

$$\theta = \frac{2(\pi - \theta_0)}{L - 2b}S + \theta_0 \tag{54}$$

Therefore, the ordinate and Abscissa of a calculated point on the pipe wall can be expressed as:

$$x(s)=\frac{L-2b}{2(\pi-\theta_0)}\times[\sin(\frac{2(\pi-\theta_0)}{L-2b}S+\theta_0)-\sin\theta_0]+b \quad (55)$$

$$x<-b, x>b$$

$$y(s)=\begin{cases} f(x) & -b\le x\le b \\ \frac{L-2b}{2(\pi-\theta_0)}\times[-\cos(\frac{2(\pi-\theta_0)}{L-2b}S+\theta_0)+\cos\theta_0]+f(b) & x<-b, x>b \end{cases} \quad (56)$$

Since the bag height H is unknown in the filling process, the filling mass W of the internal sand body can be written as a function of the bag area, which is a function of $x(s)$ and $y(s)$.

Therefore, the calculation of the shape of the film bag sandbag is a cyclic iterative process, so it is difficult to obtain a more accurate explicit expression. Via the MATLAB software, the approximate figure of the tube bag can be obtained by iterative calculation, which is shown in Figure 11.

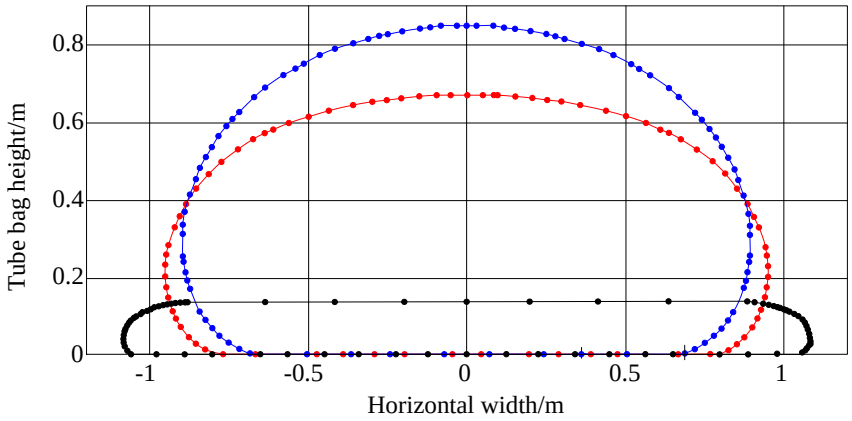

Fig. 11 Shape diagram of tube bag under different filling pressure

4. NUMERICAL STUDY OF ENGINEERING PROJECT

4.1 Engineering background

The Nacho River 2# Bridge, located in Cao Fei-Dian Industrial Zone Tangshan City, is an important traffic channel construction project connecting the North and South banks of Nacho River, and it is also the main living urban bridge in the North-South direction of the comprehensive service area of the industrial zone. The total length of the bridge is 1015.3 m, with a separate double-width girder, in which a single width of 16.5m and a reserved rail transit width of 13m in the middle. The bridge project consists of the North approach bridge (257.65m in total length of continuous beams), the main bridge (525m in total length of 7 spans continuous beams), and the South approach bridge (232.65m with a total length of 2 continuous beams). The layout and cross-section of the whole bridge are as follows.

The elevation of the normal water level at the location of the bridge is 2.7m, the low water level of the sections Pz0-Pz4 and Pz16-Pz19 is 0.3m, and the actual river bed elevation is between 2.699m and -11.791m. Since the riverbed between the piers Pz0-Pz4 and Pz16-Pz19 is relatively high, it is easy to use sand-blown cofferdams to backfill a platform, which provides a site for pile foundation construction, and can also be used as a construction access road and subsequent cast-in-suit box girder construction support foundation. The highest elevation of the cofferdam top in the backfill area is 5.05 m, and the lowest elevation is 3.2 m (Pz1 and Pz18 piers). The total length of the backfill area is 304.9 m (178.45 m on the north bank and 126.45 m on the south bank), and the top width is 52 m. The lower structure of the connection between the steel

trestle and the sand-blown cofferdam is the same as that of the trestle, and the hillside rock is replaced according to the slope of 1:1.5. The width of the top surface of the replacement is 12 m, the bottom surface of the replacement is 8 m as wide as the trestle, and the depth of the replacement is 2.4 m. The Crawler-type road rollers are used for preliminary compaction of the hillside rocks within the replacement area. The Standard section of sand blowing cofferdam is shown in Figure 12.

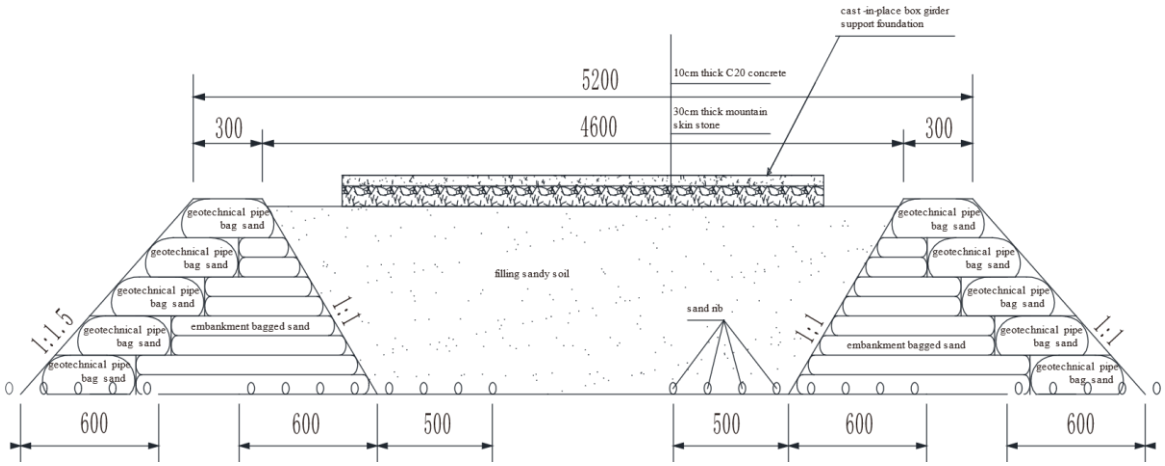

Fig. 12 Standard section of sand blowing cofferdam

The geotextile outside the mold bag sand adopts an anti-aging polypropylene geotextile bag. According to the experimental report of geosynthetics, the relevant parameters are shown in Table 1.

Table 1 Parameters of anti-aging polypropylene geotechnical mold bag

Project		Unit	Index value
Mass per unit area		g/m^2	202.3
Thickness		mm	0.2
Tensile strength	Meridian direction	N/50mm	2010
	Latitudinal direction	N/50mm	1808
Trapezoidal tear strength	Meridian direction	N	526
	Latitudinal direction	N	418
Longitude and weft density	Meridian direction	N	16
	Latitudinal direction	N	15
Elongation	Meridian direction	%	22
	Latitudinal direction	%	23
CBR bursting strength		N	4003
Peel strength		——	20
Permeability coefficient		cm/s	0.079
Equivalent aperture O_{95}		mm	0.15

According to the geological exploration data and testing reports of filled sand and geotextiles of the Nachaohe 2# Bridge in Cao Fei-Dian, Tangshan, the material parameters are listed in Table 2.

Table 2 Parameters of model sand

Materials	Natural weight γ （kN/m^3）	Internal friction angle φ （Degree）	Cohesion C （kPa）	Compression modulus E （MPa）
Silty clay	19.5	10.1	40.6	25.8
Tube bag sand	20.0	18.8	0.5	8.4
Embankment core sand	20.1	20.8	0.9	11.4

4.2 Numerical simulation results of mold bag sand

In this investigation, the general commercial finite element software ANSYS is used to establish the finite element model of the film bag sand. The mold bag sand depends on the circumferential tension of the geotechnical bag to keep its shape, which cannot be ignored in the numerical simulation calculation. When the mold bag sand is simplified to a plane element, the outer mold bag degenerates into a line element, and the contact element is used to connect the molded bag and the filling sand (Bez, et al.,2021). The detailed finite element model of pipe bag sand is shown in Figure 13.

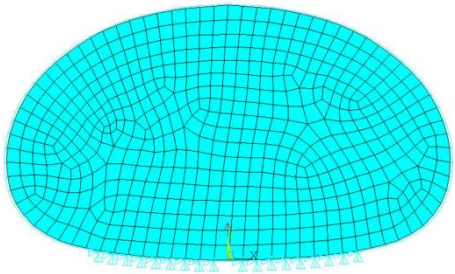

Fig. 13 Finite element model of pipe bag sand

Engineering sand and soil bodies are all rocks formed by long-term differentiation and fragmentation of the bulk structure, which is a three-phase body composed of solid, liquid and gas. In the long-term formation process affected by weathering, transport, deposition and crustal movement, the soil composition is quite complex, so the intrinsic relationship of the soil is very complex. The E-v model proposed by Duncan-Chang is used in this study, and the Mahr-Coulomb theory is used for the soil damage criterion. The model is very similar to the Mahr-Coulomb model and is called the D-P criterion in the Ansys platform. The D-P code adopts an ideal elastic-plastic model in which the damage surface does not change as the material yields, and the code can consider not only the properties of the material yield strength increase when the pressure increases, but also the properties of volume

expansion when the material yields under pressure, The detail parameter correspondence under different DP criteria can be found in Table 3, and the DP_4 criteria was employed in this investigation.

The length direction of membrane bag sand and blown sand weir is usually much larger than its width direction, and the external load on the structure is in the vertical direction, which is a typical plane strain problem, so the membrane bag sand and blown sand weir can be simplified to a plane model in the computational analysis, so Plane82 is chosen here to model the membrane bag sand and blown sand weir. Plane82 cells can be adapted to complex structure shapes, and can maintain sufficient accuracy in triangular and quadrilateral cell meshes or a mixture of the two when dividing cells. In addition, the external bag of membrane sand and the internal sand-filled body are connected by the tension and bond between the two, and the contact between the geotextile and the sand-filled body is simulated by using the point-point contact Contact12 element to simulate the contact between the line surface. In addition, the mesh of the finite element model of membrane bag sand is divided by quadrilateral free division with the size of 0.10m×0.10m.

Table 3 Parameter Correspondence under Different DP Criteria

Criterion	Relationship with Mahr Coulomb criterion	β	σ_y
DP	Hexagon outer corner circumscribed circle	$\frac{2\sin\varphi}{\sqrt{3}(3-\sin\varphi)}$	$\frac{6c\cos\varphi}{\sqrt{3}(3-\sin\varphi)}$
DP_1	Hexagon inner corner circumscribed circle	$\frac{2\sin\varphi}{\sqrt{3}(3+\sin\varphi)}$	$\frac{6c\cos\varphi}{\sqrt{3}(3+\sin\varphi)}$
DP_2	Hexagonal inscribed circle	$\frac{\sin\varphi}{\sqrt{3(3+\sin^2\varphi)}}$	$\frac{3c\cos\varphi}{\sqrt{3(3+\sin^2\varphi)}}$
DP_3	A circle equal in area to a hexagon	$\frac{2\sqrt{3}\sin\varphi}{\sqrt{2\sqrt{3}\pi(9-\sin^2\varphi)}}$	$\frac{6\sqrt{3}c\cos\varphi}{\sqrt{2\sqrt{3}\pi(9-\sin^2\varphi)}}$
DP_4	Circle matching Mahr Coulomb criterion	$\frac{\sin\varphi}{3}$	$c\cos\varphi$

4.2.1 The working condition with a cross-section height of 1m

The working condition of the finite element model of the bag sand in this study is mainly derived from the engineering practice on the construction site. The height of the bag sand is mainly divided into two categories according to the needs of the construction site: 0.5m and 1.0m. The bag sand with a height of 0.5m will also be used for the case where the upper part is covered with 2m thick soil. Considering that the height of the bag sand is 0.5m and 1.0m respectively, on the other hand, it can also verify the correctness of the theoretical formula

derivation in section 2 of this investigation，as well as the comparison between the specific theoretical analysis and finite element simulation results can been found in the following chapters.

For the tube bag sand, the relationship between its section height and the tension of the geomembrane bag outside the tube bag is analyzed via numerical calculation. For the working condition with a section height of 1m, the calculation results are shown in Figure 14.

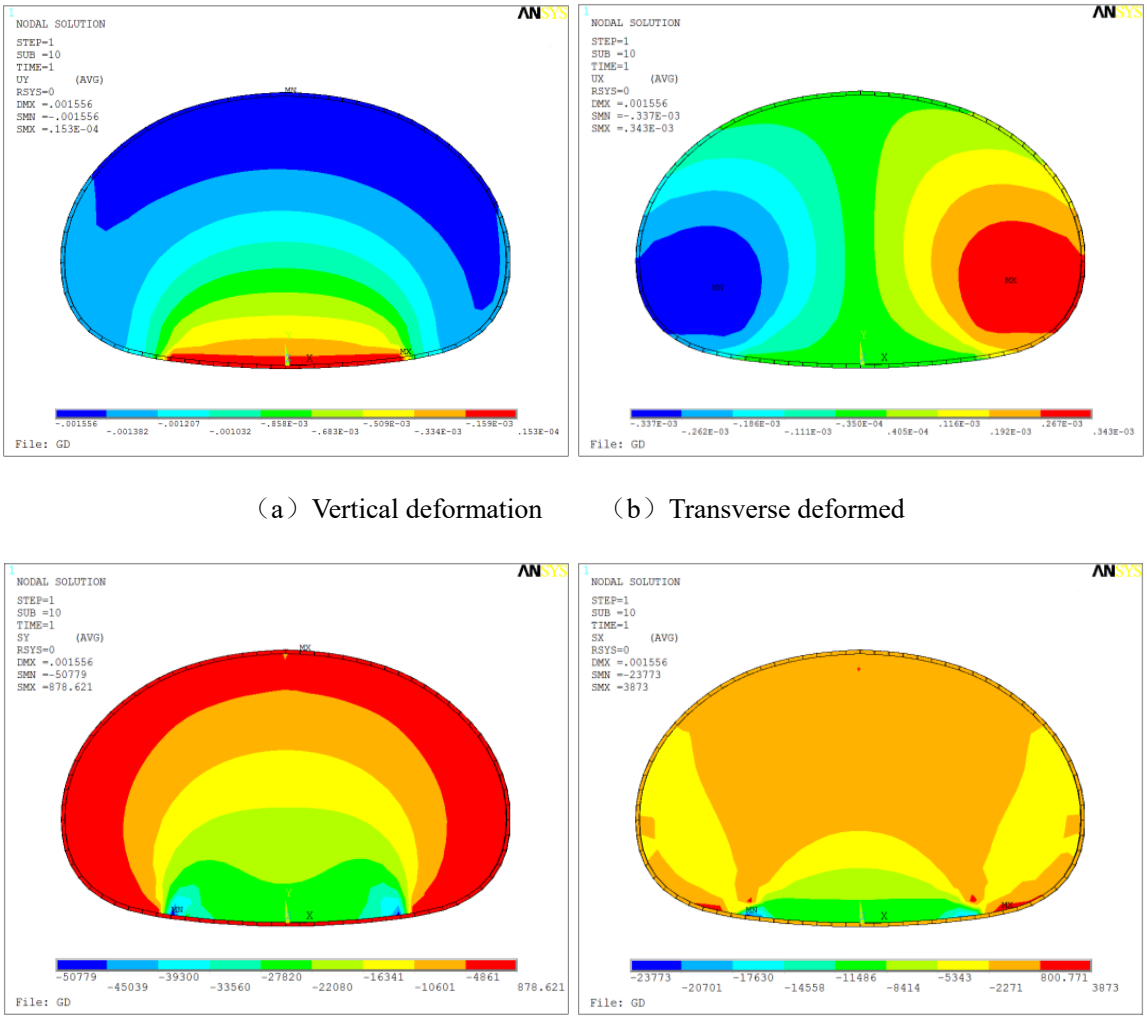

（a）Vertical deformation （b）Transverse deformed

（c）Vertical stress （d）Transverse stress

Fig. 14 Calculation results under the gravity with a cross-section height of 1m

It can be seen from the Figure 14 that only under gravity, the maximum vertical deformation of mold bag sand with a 1m height cross-section is 1.6 mm, which occurs on both above sides of the mold bag sand. The vertical deformation decreases with the decrease of the height of the bag sand. Because the contact constraint condition is set at the bottom of the bag sand, the bottom deformation is only 0.01 mm, which can be almost ignored. In terms of transverse deformation, the maximum transverse deformation of the bag sand on the left side is 0.34mm. From

left to right, the transverse deformation of the bag sand first decreases and then increases, and the maximum deformation on the right side is 0.27mm. In general, the transverse deformation presents a significant trend of large on both sides and small in the middle.

The change nephogram of vertical and transverse stress of the bagged sand are shown in the Figure 14 (c) and (d), respectively. Due to the stress concentration and distortion at the constraint position of the boundary conditions, the stress in the whole boundary area cannot reflect the stress distribution law of the bagged sand. After deducting this part, it can be seen that the vertical stress of the bagged sand gradually decreases from top to bottom, with the maximum effective stress of 27.8Mpa and the minimum effective stress of 10.6Mpa; For the transverse stress of bag sand, there is also local stress and the distortion of the whole boundary. Therefore, the transverse stress also shows a decreasing trend from top to bottom. The maximum and minimum transverse effective stresses are 11.5Mpa and 2.3Mpa respectively. At this time, the strain value of the outer geomembrane bag is 0.106 and the axial force is 4.68 KN. Only under the dead load, the circumferential pulling force of the sandbag is: $T = \gamma \frac{H^2}{4} = 20KN/m^3 \times \frac{1}{4} m^2 = 5KN/m$.

It can be seen that the above equivalent calculation formula is consistent with the numerical simulation results. From the deformation results, it can be seen that under the gravity, the longitudinal and transverse deformation on both sides of the tube bag is large, and the transverse stress is large, which is the disadvantageous position of the tube bag sand.

4.2.2 The working condition with a cross-section height of 0.5m

For the condition that the cross-section height of 0.5m, the corresponding calculation results are shown in Figure 15.

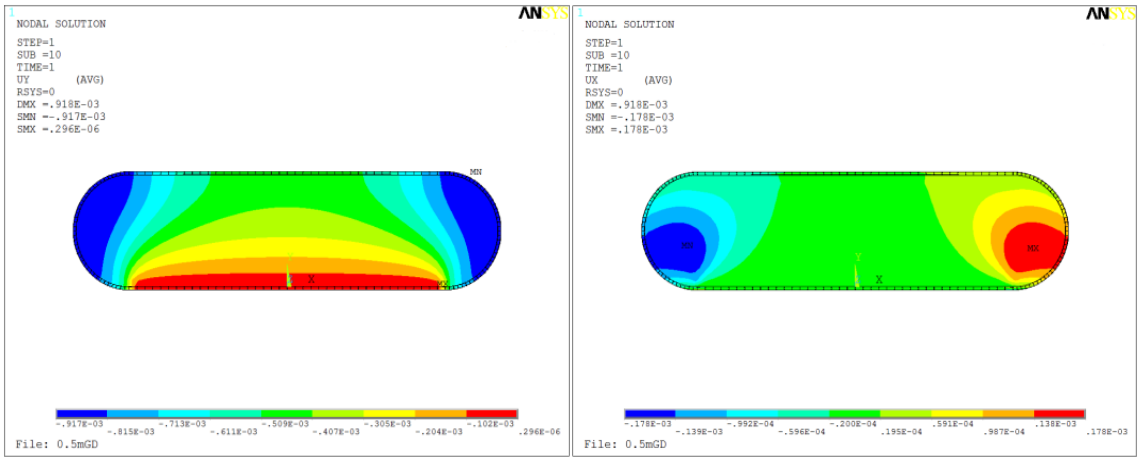

（a）Vertical deformation （b）Transversely deformed

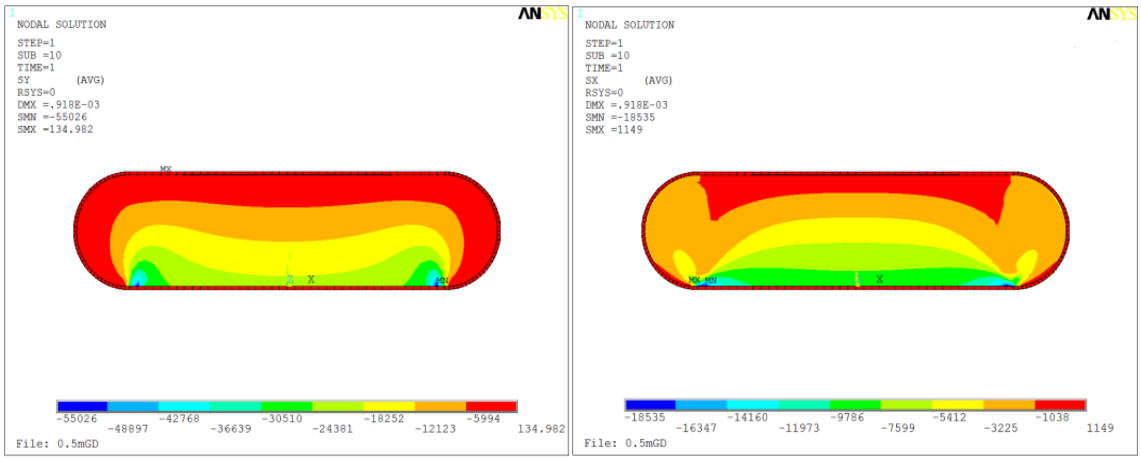

(c) Vertical stress (d) Transverse stress

Fig. 15 Calculation results under the gravity with a cross-section height of 0.5m

It is seen that the maximum vertical deformation of the 0.5 m height mold bag sand is 0.92 mm only under the gravity, which is generated on both above sides of the mold bag sand, and the maximum lateral deformation is 0.17 mm. Similar to the working condition with a cross section height of 1m, the vertical deformation of this working condition decreases with the decreasing of the height of the bag sand. Since the total height of the bag sand is only 0.5m, the vertical deformation is also far less than that under the working condition with a cross section height of 1m. In terms of transverse deformation, the maximum transverse deformation of the bag sand on the left side is 0.17mm. From left to right, the transverse deformation of the bag sand first decreases and then increases, and the maximum deformation on the right side is 0.14mm.

Excluding the position of boundary stress distortion, the maximum vertical compressive stress is 30.5 KPa, and the maximum transverse stress is 9.79 KPa. At this time, the circumferential force of the outer geomembrane bag is 1.43 KN. Only under the dead weight load, the circumferential pulling force of the sandbag is $T = \gamma \frac{H^2}{4} = 20kN/m^3 \times \frac{0.5^2}{4} m^2 = 1.25kN/m$.

Figure 15 (c) and (d) shows the vertical and horizontal stress nephogram of the bagged sand under this working condition, which is similar to Figure 14. Due to the stress concentration and distortion at the constraint position of the boundary conditions, the stress in the whole boundary area cannot reflect the stress distribution law of the bagged sand. After deducting this part, it can be seen that the vertical stress of the bagged sand gradually decreases from top to bottom, with the maximum effective stress of 30.5Mpa and the minimum effective stress of

12.1Mpa; For the transverse stress of bag sand, there is also local stress and the distortion of the whole boundary. Therefore, the transverse stress also shows a decreasing trend from top to bottom. The maximum and minimum transverse effective stresses are 9.8Mpa and 3.2Mpa respectively.

4.2.3 The height of the section is 0.5m with an external load.

Considering there are 0.5m high mold bag sand with the 2m high covering soil, the calculation result is shown in Figure 16.

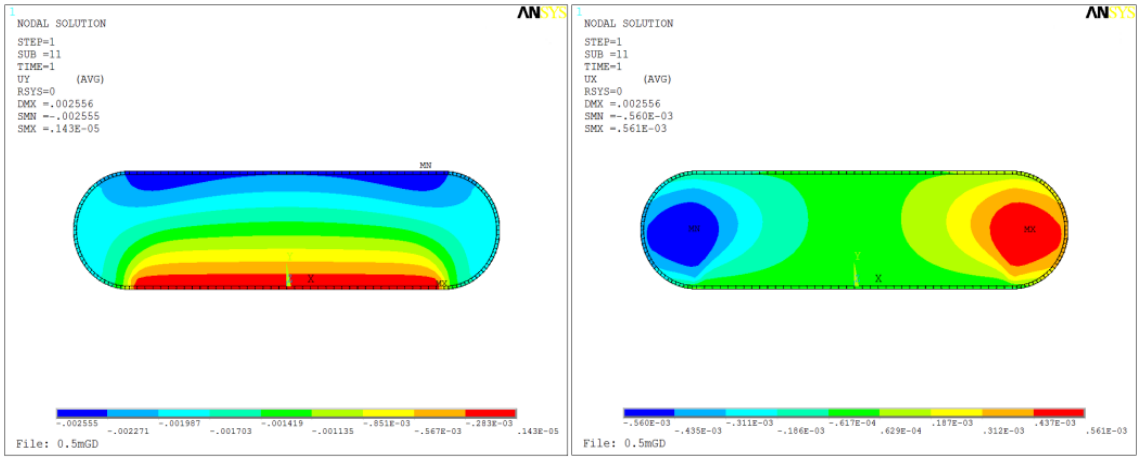

（a）Vertical deformation （b）Transversely deformation

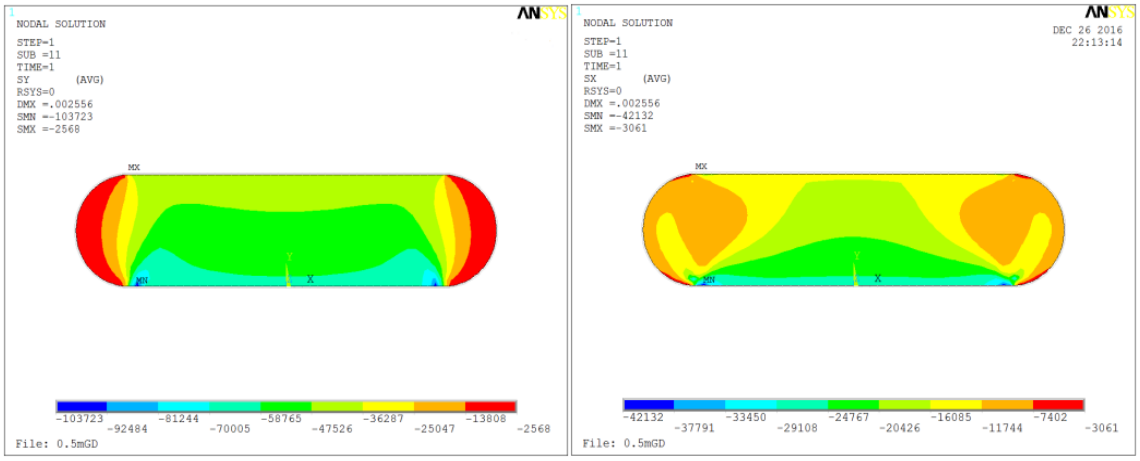

（c）Vertical stress （d）Transverse stress

Fig. 16 Calculation results of 0.5m high mold bag sand under dead weight and external load

When the 0.5m high mold bag sand with the 2m high covering soil to be considered, the maximum vertical deformation is 2.6 mm, which occurs on both above sides of the mold bag sand. Compared with the dead weight of the bag sand with the height of 0.5m, the vertical deformation of the bag sand is significantly increased by

283% after the soil covering load is considered. The maximum lateral deformation on the left side is 0.56mm, and the maximum deformation on the right side is 0.44mm. The increase is also very significant.

After deducting the stress concentration and distortion at the constraint position of the boundary conditions, the vertical stress of the bag sand under this working condition gradually decreases from top to bottom, with the maximum effective stress of 81.2Mpa and the minimum effective stress of 36.3Mpa; For the transverse stress of bag sand, there is also local stress and the distortion of the whole boundary. Therefore, the transverse stress also shows a decreasing trend from top to bottom. The maximum and minimum transverse effective stresses are 33.5Mpa and 16.1Mpa respectively. At this time, the force of the outer geomembrane bag is 9.8 KN.

4.2.4 Comparative analysis of theoretical and simulated values of membrane bag under typical working conditions

In order to compare and analyze the similarities and differences between the theoretically values of the displacement deformation and stress response of the membrane bag under typical working conditions and the numerical simulation results, in this part, the response values of the cross-sectional height of membrane bag of 1.0 m and 0.5 m under gravity, as well as response values of the section height of 0.5m under gravity and external load are listed in Table 4.

Table 4 The theoretical and simulated values of the displacement and stress of the film bag sand under typical working conditions

Case name	Maximum vertical deformation			Maximum Lateral deformation		
	Theoretical value (mm)	Simulated value (mm)	Relative error (%)	Theoretical value (mm)	Simulated value (mm)	Relative error (%)
Cross-section height of 1.0 m under gravity	1.45	1.60	10.34%	0.39	0.34	12.82%
Cross-section height of 0.5 m under gravity	0.88	0.92	4.55%	0.15	0.17	13.33%
Cross-section height of 0.5 m under gravity and external load	2.78	2.60	6.47%	0.59	0.56	5.08%
Case name	Maximum vertical stress			Maximum Lateral stress		
	Theoretical value (kPa)	Simulated value (kPa)	Relative error (%)	Theoretical value (kPa)	Simulated value (kPa)	Relative error (%)
Cross-section height of 1.0 m under gravity	30.45	27.80	8.70%	12.21	11.50	5.81%
Cross-section height	32.50	30.50	6.15%	8.89	9.79	10.12%

of 0.5 m under gravity						
Cross-section height of 0.5 m under gravity and external load	90.42	81.20	10.20%	37.53	33.50	10.74%

From the comparison results in Table 3, it can be seen that whether it is displacement deformation or stress response, the theoretical analysis results of the membrane bag are basically consistent with the numerical simulation calculation results. The maximum error is 13.33%, which is controlled within 15%, which means the calculation accuracy can meet the requirements of engineering practice. The main reason for the existence of certain errors is that the working conditions and cross-sectional shape of the film bag sand are simplified to a certain extent in the process of theoretical analysis, which is different from the actual situation of engineering, thus making the theoretical value has a certain error with the analog value. It can be seen from Figure 3 that the maximum stress and deformation simulation values in vertical and horizontal directions under various working conditions are greater than the theoretical values, and the minimum relative error is 4.55%. The analysis of the reasons for the error is mainly due to the differences between the constitutive model, element type and analytical theoretical model of the membrane sand material in the numerical simulation. In addition, the size of the grid division has a certain impact on the results of the numerical simulation, However, too small grid division will cost a lot of calculation time. Considering the calculation time and accuracy, the relative error of this study is acceptable.

4.2.5 Analysis of the influence of concrete Slab thickness on settlement

The commonly used calculation methods for foundation settlement include elastic theory formula and one-way compression method. However, the conventional calculation methods are based on the semi-infinite lifting assumption, that is, the foundation is infinitely wide below the foundation. However, as the foundation of cast-in-situ continuous beam, the sand blowing cofferdam cannot satisfy the semi-infinite body assumption, so the commonly used sand settlement calculation method is no longer applicable. This section uses ANSYS finite software to calculate the cofferdam settlement under full support load based on the measured material characteristics. The span of the north bank approach bridge of Cao Fei-Dian Nacho River 2# Bridge is 39.5m+49.5m+39.5m=128.5m, the section height of the side pier support is 1.6m, the section height of the middle pier support is 2.7m, the middle section height of the main span is 2.0m, and the bottom plate of the box girder

changes according to the quadratic curve.

In order to simplify the calculation, the mold bag sand on both sides of the sand blowing cofferdam is equivalent to a rectangle, and the section is divided into three parts: flange and box chamber. The dead weight of the box girder and the weight of the support are converted into the sectional uniform line load. The average line load of the flange of the middle pier section and the box type is and respectively, and the average line load of the midspan section is and respectively. The calculation model is shown in Figure 17.

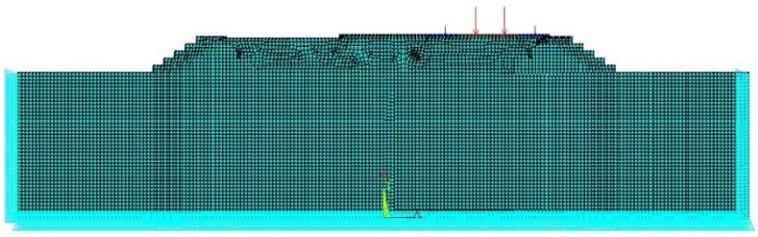

Fig. 17 Overall Calculation Model of Cofferdam

Under gravity and external load f_P, the conversion values of sand cohesion of pipe bags with different buried depths are listed in Table 5.

Table 5 Conversion cohesion value of mold bag sand

Inside	1	2	3	4	5	6	7	8
Converted value（kPa）	6.85	9.23	11.61	13.99	16.37	18.7	23.51	25.89
Outside	1	2	3	4	5			
Converted value（kPa）	6.89	14.87	18.06	18.06	18.06			

For the cast-in-suit concrete slab with a thickness of 0.1m, the results calculated by ANSYS finite element software are as shown in Figure 18.

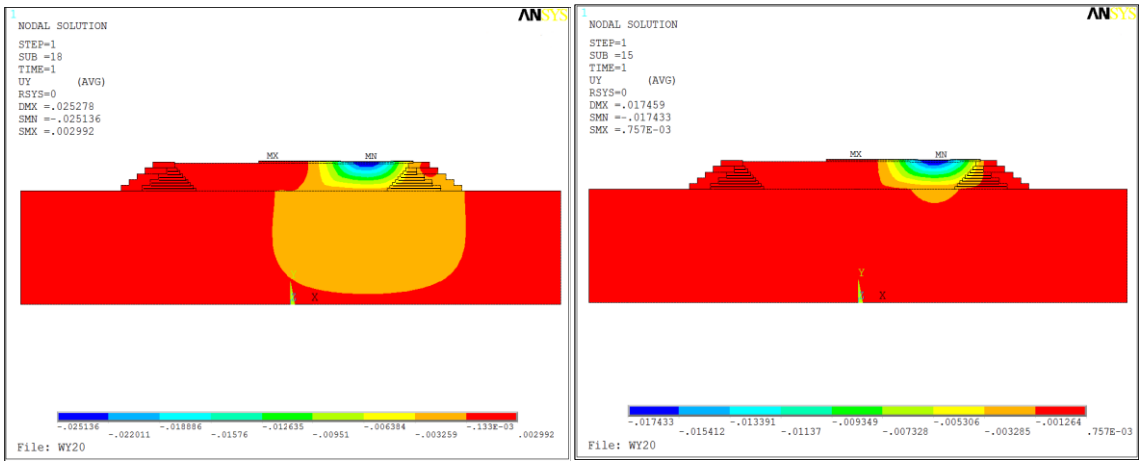

（a）Vertical deformation (middle pier section)（b）Vertical deformation (mid-span section)

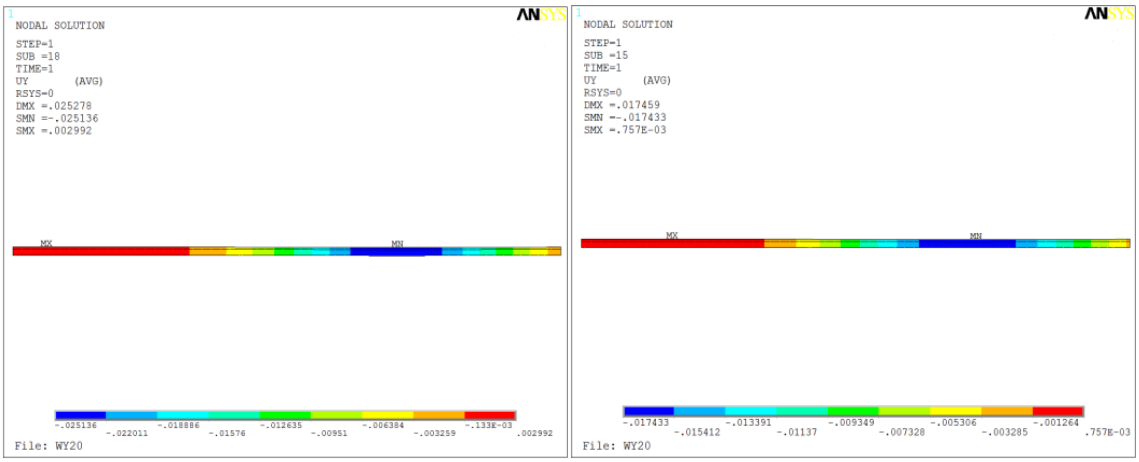

（c）Transverse deformation (middle pier section)（d）Transverse deformation (mid-span section)

Fig. 18 Calculation result with 0.1m thick concrete slab settlement s (unit: m)

It can be seen that when the cast-in-suit concrete slab thickness is 0.1m, the sand-blown cofferdam is under the load of the full hall support, at the section of the middle pier, the maximum vertical settlement is 24.2 mm, and the maximum lateral settlement difference is 21.0 mm. When the maximum vertical settlement difference is 17.1 mm, the lateral maximum settlement difference is 14.0 mm.

For the cast-in-suit concrete slab thickness of 0.15m, the calculation results via ANSYS finite element software are shown in Figure 18.

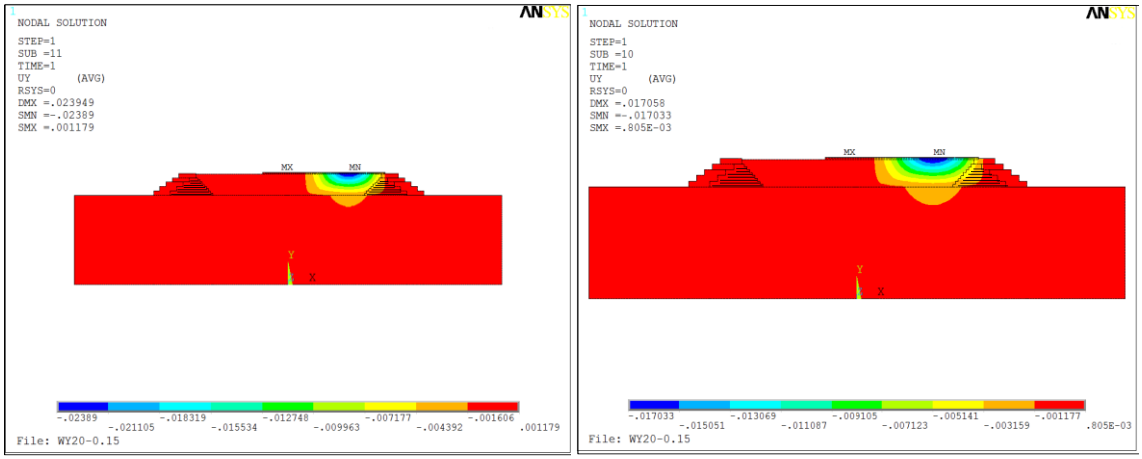

（a）Vertical deformation (middle pier section)（b）Vertical deformation (mid-span section)

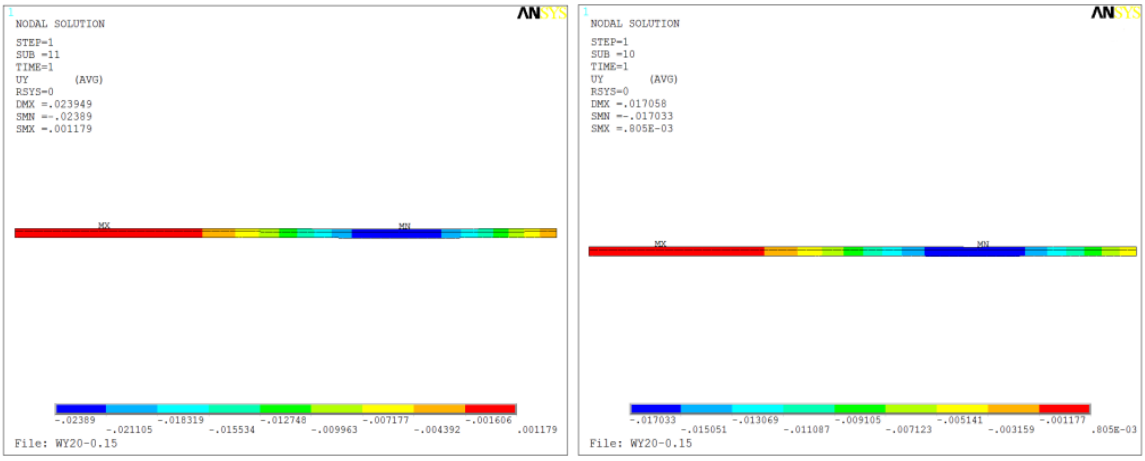

（c）Transverse deformation (middle pier section)（d）Transverse deformation (mid-span section)

Fig. 18 Calculation results with 0.15m thick concrete slab settlement (unit: m)

When the thickness of cast-in-suit concrete slab is 0.15m, the sand-blown cofferdam is under the load of the full hall support, at the section of the middle pier, the maximum vertical settlement is 23.9 mm, and the maximum lateral settlement difference is 19.5 mm. When the vertical maximum settlement difference is 17.0 mm, the lateral maximum settlement difference is 14.0 mm. The settlement calculation results under other conditions are shown in the following Figure 19.

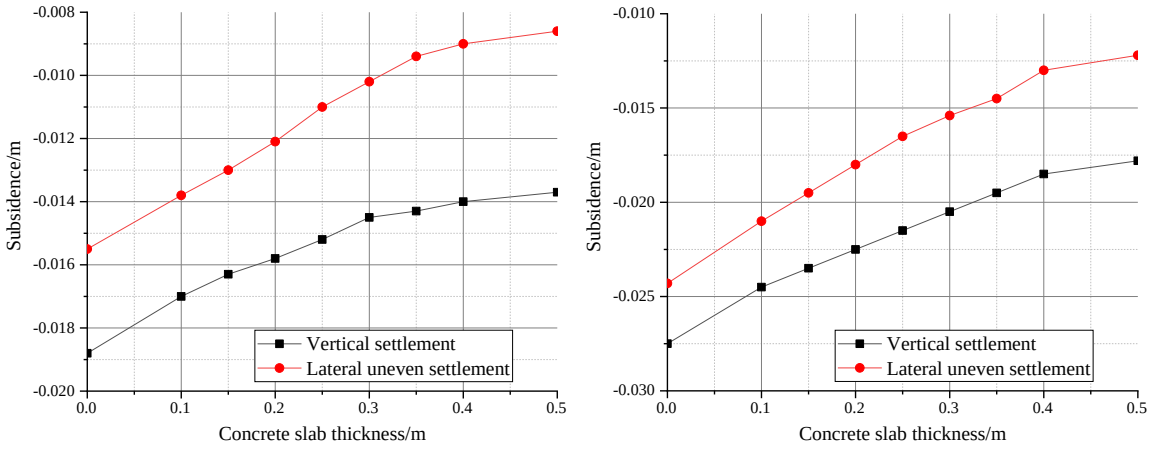

（a）the section at the midspan　　（b）the section at middle pier

Fig. 19 Calculation result of weir settlement

It can be seen with the increasing of the thickness of the concrete slab, the vertical maximum settlement of the cofferdam decreases gradually, and the uneven settlement of the transverse bridge also decreases gradually. Moreover, it can be seen that the reduction of lateral uneven settlement is greater than the reduction of vertical settlement, and the increase of concrete slab thickness has a significant effect on reducing the lateral settlement. At the same time, it can be seen from the calculation results that when the concrete slab thickness increases from 0m

to 0.5m, the maximum vertical settlement decreases by 0.01m. It can be seen that increasing the concrete slab thickness to reduce the settlement is effective, but blindly increasing the slab thickness is not economical. Therefore, the thickness of the concrete slab should be reasonably selected during the construction process.

5. CONCLUSIONS

Aiming to solve the limitations of the current research on membrane bag sand, this paper deduces the relationship between the height of the membrane bag sand body and the tension of the geotechnical sandbag through theoretical calculations and further proposes the shape of the sandbag and the relationship between its weight and external load. Also through theoretical calculation, it is verified that the effect of the hoop action of the geotextile bag on the filling sand on the overall shear strength of the internal sand body. The main conclusions are as follows:

(1) The effect of the geotextile bag on the hoop of the sand-filled inside is equivalent to providing an additional cohesion c_f to the sandy soil, which increases the overall shear strength. For non-cohesive soil, the role of the geotextile bag is mainly to make the contact pressure between the sand particles increase, as well as the first and third principal stresses of the sand body element increase, thereby making the overall shear strength increase.

(2) After ignoring the friction between the geotechnical sandbag and the filling sand, the shape of the piping bag can be approximated and simplified to an expression related to the filling pressure, the deadweight load of the sand body, and the boundary conditions of the foundation; combined with the equivalence cohesion formula, the equivalent calculation formula for the strength of the soil body under different burial depth conditions is obtained, so that the cofferdam can be equated to a variety of materials according to the different burial depths when the cofferdam calculation is carried out, avoiding the defects that existed in the previous single material calculation.

(3) Based on the ANSYS finite element software, a simplified model of molded sand and blown sand cofferdam is established based on the measured material parameters, and the axial tension of the molded sand geomembrane bag is calculated for different pipe bag heights and under the dead weight and external

load, and the change law of blown sand cofferdam at different concrete slab thicknesses is analyzed. Through numerical simulation, it is known that the axial tension of the molded bag is proportional to the second power of the height of the mold bag sand without considering the friction condition, which is consistent with the theoretical formula.

(4) It can be seen that whether displacement deformation or stress response, the theoretical analysis results of the membrane bag are basically consistent with the numerical simulation calculation results. The maximum error is 13.33%, which is controlled within 15%, which means the calculation accuracy can meet the needs of engineering practice. With the concrete slab thickness increasing, the vertical settlement of the blown sand cofferdam gradually decreases under the action of the cast-in-suit bracket, and the degree of reduction of the uneven settlement in the cross-bridge direction is more obvious than that of the vertical settlement.

DATA AVAILABILITY

The data used to support the findings of this study are available from the corresponding author upon request.

CONFLICTS OF INTEREST

The authors declare that they have no conflicts of interest.

ACKNOWLEDGMENTS

The research reported in this paper was supported by China Natural Science Foundation (No. 51778532 and 52008047), Their support is gratefully acknowledged.

REFERENCES

Bensmaine, A., Benmebarek, N., & Bensmebarek, S. (2022). “Numerical Analysis of Seepage Failure Modes of Sandy Soils within a Cylindrical Cofferdam. ”Civil Engineering Journal, 8(7), 1388-1405.

Bez, A., Bedon, C., Manara, G., Amadio, C., & Lori, G. (2021). Calibrated numerical approach for the dynamic analysis of glass curtain walls under spheroconical bag impact. Buildings, 11(4), 154.

Chen, L., & Jeng, D. S. (2022). “Study on the seabed response around a dumbbell cofferdam under combined wave and current loading”. Ocean Engineering, 256, 111456.

Chen, L. W., Zhou, X. W., Gong, B. W., Li, B. and Tong, J., (2016). “Centrifugal modeling of big sandbag cofferdam on coastal soft soil.” Chinese Journal of Rock Mechanics and Engineering, 4235-4240.

Guo, W., Chu, J., Yan, S., (2011). “Effect of subgrade soil stiffness on the design of geosynthetic tube.” Geotextiles and Geomembranes, 29(3): 277-284.

Kang, A., Zhu, B., Lin, P. Z., Ju, J. W., Zhang, J. W. and Zhang, D. M., (2020). “Experimental and numerical study of wave-current interactions with a dumbbell-shaped bridge cofferdam.” Ocean Engineering, 210: 107433.

Lambe, T. W. and Whitman, R. V. , (1991). “Soil mechanics.” John Wiley & Sons.

Liu, A., Liang, A., (2016). “Comprehensive application of geosynthetics in solidified soil sea dike projects.” Chinese Journal of Geotechnical Engineering, 38(S1): 177-180. (in Chinese)

Liu, A. M., Li, B. and Tong, X. Y., (2020). “Research on Deformation Characteristics of New Type of Cofferdams Structure.” The 30th International Ocean and Polar Engineering Conference. OnePetro, 1730-1733.

Li B. (2019). “Simulation and Analysis of Deformation Characteristics of Moulded Bag Solidified Soil Embankment.”IOP Conference Series: Earth and Environmental Science. IOP Publishing, 242(6): 062023.

Liu, W. C., Zhang, Y. P., Li, T. and Yu, Y. N., (2010). “Simulation of filling construction of permeable geosynthetic tubes.” Journal of Zhejiang University-Science A, 11(6): 425–431.

Li, D., Wu, D. S., Xu, F. G., Lai, J. H. and Shao, L., (2018). “Literature overview of Chinese research in the field of better coal utilization.” Journal of Cleaner Production, 2018, 185: 959-980.

Lu, X., Luo, Y., Ming, H., Zhou, M., Zhang, X., & Liu, D. (2023). “Stability of Nonuniform Large Geotextile-Reinforced Cofferdam under Seepage and Excavation Effects.” International Journal of Geomechanics, 23(2), 04022283.

Malik, J., Sysala, S., (2011). “Analysis of geosynthetic tubes filled with several liquids with different densities.” Geotextiles and Geomembranes, 29(3): 249-256.

Matsuoka, H., (2003). “Tribology in soilbag.” Journal of Japanese Society of Tribologists, 48(7): 547−552.

Matsuoka, H. and Liu, S. H., (2006). “A new earth reinforcement method using soil bags.” London: Taylor &

Francis, 173-188.

Namias, V., (1985). 'Load-Supporting Fluid-Filled Cylindrical Membranes." Journal of Applied Mechanics, 12:913-918.

Plaut, R. H. and Klusman, C. R., (1999). "Two-dimensional analysis of stacked geosynthetic tubes on deformable foundations." Thin-Walled Structures, 34(3): 179-194.

Peng, W., Chen, L. and Zhou, X., (2018). "Application of Large-Size Sandbag Cofferdam in Land Reclamation Engineering." GeoShanghai International Conference. Springer, Singapore, 271-278.

Pei, J., Einstein, H. H. and Whittle, A. J., (2018). "The normal stress space and its application to constructing a new failure criterion for cross-anisotropic geomaterials." International Journal of Rock Mechanics and Mining Sciences, 106: 364-373.

Restall, S. J., Jackson, L. A., Heerten, G. and Hornsey, W. P., (2002). "Case studies showing the growth and development of geotextile sand containers: an Australian perspective." Geotextiles & Geomembranes, 20(5):321-342.

Saathoff, F., Oumeraci, H. and Restall, S., (2007). "Australian and German experiences on the use of geotextile containers." Geotextiles & Geomembranes, 25(4-5):251-263.

Wang, T. T., Liang, H.and Peng, Z. H., (2020). "Numerical simulation on offshore artificial island cofferdam of Hong Kong-Zhuhai-Macao Bridge." International Journal of Computer Applications in Technology, 62(4): 285-295.

Xiu, C., Lu, X., Huo, S. X., Li, Z. X., Ma, T. and Chen, K., (2021). "Discussion on the Evolution of Sea Reclamation from 2006 to 2018 in Jimo District, Qingdao, Shandong Province." Earth and Environmental Science, 658: 012031.

Xue, R., Bie, S., Guo, L. L. and Zhang, P. L., (2019). "Stability analysis for cofferdams of pile wall frame structures." KSCE Journal of Civil Engineering, 23(9): 4010-4021.

Yang, M. J., Zang, D. and Liu, L., (2009). "Application of sand-bag cofferdam by hydraulic filling for NANJMAT project in UAE." China Harbour Engineering, 3: 45-48. (in Chinese)

Zhou, X. W., Wang, X. L., Wang, M. Y. and Wang, L., (2017). "Characteristics of failure zones of soft soil foundation under flexible load sandbag cofferdam." Chinese Journal of Geotechnical Engineering,

39(z2): 45. (in Chinese)

Zhou, X., Wang, L., Wu, L. and Lin, R., (2014). “Analysis of stability of dykes with fibriform sand on the soft foundation.” Journal of Hohai University (Natural Sciences), 03.